PHY6000 | PV SYSTEMS

A Comparative Analysis of All-Perovskite and III-V Multijunction Photovoltaics for Terrestrial and Space Applications

Dinesh Behera

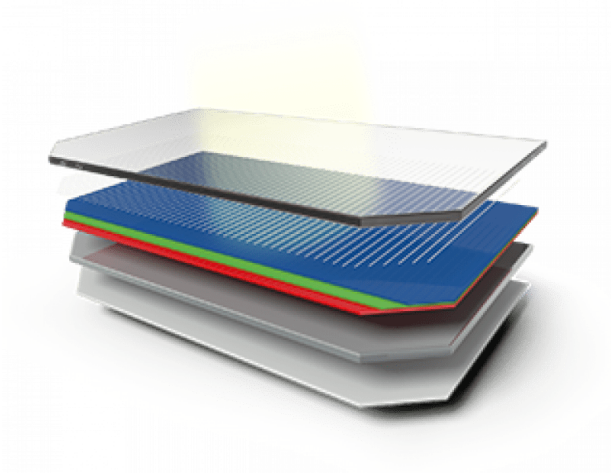

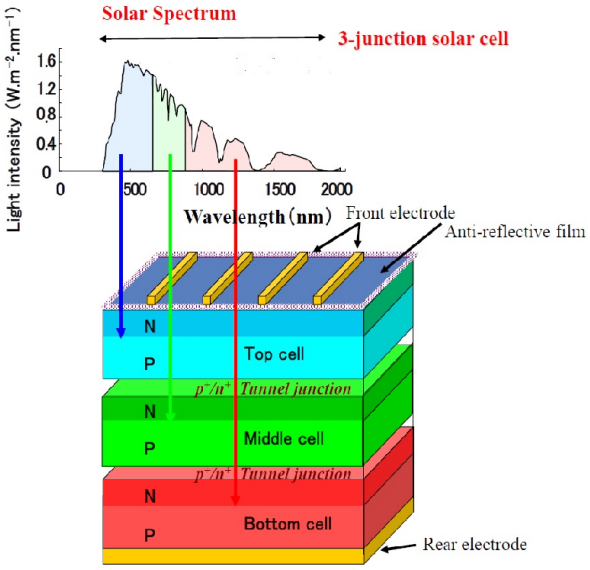

INTRODUCTION

Photovoltaic devices are not only essential for generating power on Earth but also play a pivotal role in guaranteeing the smooth functioning of space missions, satellites, and the International Space Station (ISS) within the demanding outer space environment. Ongoing research in photovoltaics concentrates on fine-tuning the performance triangle, encompassing power conversion efficiency (PCE), stability, and production cost. In the realm of space photovoltaics, critical considerations comprise achieving high efficiency, radiation resistance, durability, lightweight design, embracing technological advancements, adapting to evolving regulations, and promoting sustainability.[1]

In Photovoltaics, theoretical detailed balance calculations impose a limit on single junction solar cells, indicating a maximum achievable PCE of 33.7%. This efficiency peak is anticipated when the bandgap energy reaches approximately 1.34 eV.[2] Nevertheless, a strategy to surpass the

PCE limitation involves mitigating short-circuit current density (J_{SC}) losses and increasing the open-circuit voltage (V_{OC}) by incorporating multiple light-absorbing layers with complementary bandgaps. These devices are tandem solar cells (two junctions - 2J) and multijunction solar cells (3J or more). The tandem solar cell devices are available in two architectures, one is a 4-terminal device (stacked tandem architecture) and the other is a 2-terminal device (monolithic tandem architecture). The 4-terminal device extracts the most power theoretically, however, it requires independent contacts to be made to the top and bottom cells, which is difficult to do in practice. Hence, 2-terminal devices are preferred where only the V_{OC} is enhanced and is given by the sum of the V_{OC}s of the cells in the stack.[3]

The historical evolution of space photovoltaics demonstrates a gradual improvement in efficiency, transitioning from silicon-based cells in the late 1950s to the adoption of III-V multijunction solar cells in the 1990s.[4] A significant milestone was the introduction of triple-junction cells utilizing Gallium Indium Phosphide (GaInP) and Gallium Arsenide (GaAs).

Tandem and multijunction devices in the current scenario are mostly based on III-V semiconductors, incorporating ternary alloys to enable band-gap tuning through precise composition engineering. GaAs, a binary semiconductor possessing favorable material and carrier transport properties, is common. GaAs can be seamlessly grown onto GaInP without significant complications related to lattice strain. Multijunction solar cells, based on GaAs and GaInP, have demonstrated impressive potential in 2J, 3J, and 4J configurations, achieving notable power conversion efficiencies (PCEs) of approximately 31%, 38%, and 39%, respectively, under standard terrestrial conditions.[5] Despite these accomplishments, the manufacturing processes essential for these crystalline, lattice-matched multijunction solar cells—such as metal-organic chemical vapor deposition (MOCVD) or molecular beam epitaxy (MBE)—remain notably expensive. This cost challenge poses a barrier to the widespread adoption of these high-performance solar cells in terrestrial applications and hence III-V multijunction PV devices are mostly used for space applications.[4]

Remarkably, the implementation of III-V semiconductor-based multijunction PV technologies has significantly increased efficiency and overall performance. GaAs-based multijunction photovoltaic cells, in particular, stand out in space photovoltaics due to their outstanding radiation resistance and efficiency.[1] Furthermore, the utilization of thin-film and flexible solar cells has introduced new possibilities for power generation on small satellites. Despite their high performance, multi-junction III-V PV technologies have drawbacks, including rigidity, thickness (80 to 200 μm), weight, and complex fabrication processes.[4]

Perovskites, characterized by their ABX_3 crystal structure, exhibit significant promise in tandem and multijunction solar cell devices due to their broad range tunable bandgap, low-cost solution-based fabrication, high efficiency, high tolerance to defects, high specific power (23 W g^{-1}), and exceptional radiation tolerance.[6,7] These appealing attributes position perovskites as attractive absorbers not only for terrestrial applications but also for space applications. By selecting specific components—A = (Cs, MA or FA), B = (Sn or Pb), and X = (I, Br or Cl)—the bandgap of perovskites can be finely tuned across a range from 1.2 eV to 3.5 eV.[8] This tunability

is particularly crucial for their effectiveness in tandem and multijunction solar cells. Research by Maximilian T. Hörantner et al. has underscored that perovskite-based tandem and multi-junction devices hold the potential to surpass the performance records set by III-V semiconductor-based tandem and multijunction solar cells.[9]

Despite being rigid and heavy (0.4-0.8 W g^{-1}), III–V semiconductor-based multi-junction solar cells stand out as the preferred choice for space solar cell technologies. Their outstanding performance, commercially available with approximately 32% PCE, and impressive resilience to radiation (retaining PCEs of around 87-90% after exposure to electron or proton irradiation) make them the primary option. Currently, the cutting-edge technology for space photovoltaics involves the triple junction comprising $Ga_{0.50}In_{0.50}P/Ga_{0.99}In_{0.01}As/Ge$ on a Ge substrate.[1,4]

Lead-based I/Br mixed-halide perovskites, denoted as $APb(I_{1-x}Br_x)_3$, showcase bandgap variations from 1.5 to 2.4 eV with increasing x. This bandgap range positions these mixed-halide perovskites as suitable wide bandgap (WBG) absorbers for tandem and multijunction devices.[10]

However, the pursuit of optimal bandgaps encounters challenges due to the inherent instability of compositions, hindering WBG absorbers from achieving comparable power conversion efficiencies (PCEs) as their bottom cell counterparts. The low PCEs of WBG solar cells can be attributed to voltage losses (V_{OC} losses) resulting from light-induced phase segregation or halide segregation, known as the Hoke effect.[11] Halide segregation occurs in mixed-halide perovskite films, leading to the formation of iodide-rich and bromide-rich phases. These iodide-rich phases exhibit lower bandgaps than the surrounding material, consequently limiting the V_{OC} of the solar cell. Although efforts are underway to address this issue, and progress has been made in mitigating the problem, there is still room for improvement.[10,12]

As Bingcheng Yu et al. suggest inorganic perovskite materials showcase higher thermal and light illumination stabilities than hybrid organic-inorganic perovskites, Cs-based mixed halide perovskites, which feature smaller A-site cations and higher iodide anion content, exhibited greater lattice distortion and superior stability under illumination compared to hybrid organic-inorganic perovskites. However, for 2.0-eV-bandgap Cs-based mixed halide perovskites, such as $CsPbI_{1.4}Br_{1.6}$ as the top cell absorber in the multijunction devices, one still encounters the issue of phase segregation to some extent when exposed to light.[13–15]

However, recent research work by Zaiwei Wang et al. has focused on suppressing halide segregation through compositional engineering of such Cs-based inorganic I/Br mixed-halide perovskites. Their findings suggest a positive correlation between increasing lattice distortion in the perovskites, achieved through rubidium (Rb) alloying to A-site cation, and the successful suppression of phase segregation.[14] Through this numerical analysis, the novel wide bandgap perovskite and the triple junction solar cell device introduced by Wang et al. will be studied.

Objective

This study aims to compare and analyse the performances of $CsPbI_{1.4}Br_{1.6}$, and $Rb_{0.15}Cs_{0.85}PbI_{1.75}Br_{1.25}$ as wide bandgap absorbers in the multijunction devices, and further

compare and analyse the commercially well-established $Ga_{0.50}In_{0.50}P/Ga_{0.99}In_{0.01}As/Ge$ and novel (2-eV-Rb-Cs-mixed-halide-perovskite)/(1.6-eV-perovskite)/(1.22-eV-Sn-Pb-mixed-perovskite) multijunction devices under standard terrestrial (AM1.5G) and standard extraterrestrial conditions (AM0).

METHODOLOGY

In 2000, the American Society for Testing and Materials (ASTM) developed the ASTM E-490 air mass zero reference spectrum for the aerospace community. This solar spectral irradiance is based on diverse data sources such as satellites, space shuttle missions, high-altitude aircraft, rocket soundings, and ground-based solar telescopes. The integrated spectral irradiance adheres to the solar constant value acknowledged by the space community, set at 1366 W/m².[16]

Simultaneously, in collaboration with ASTM and government laboratories, the photovoltaic sector established two standardized terrestrial solar spectral irradiance distributions. These distributions cover the AM1.5 Global spectrum, tailored for flat plate modules with an integrated power of 1000 W/m² (100 mW/cm²), and the AM1.5 Direct (+circumsolar) spectrum, designed for solar concentrator applications. The latter comprises the direct beam from the sun along with the circumsolar component within a 2.5-degree disk around the sun, resulting in an integrated power density of 900 W/m². Both reference spectra are consolidated into a singular document, ASTM G-173-03, which can be found on the NREL website. This compilation ensures consistent solar radiation characterisation, serving as a vital industry benchmark for applications like concentrated solar power and photovoltaic systems.[17]

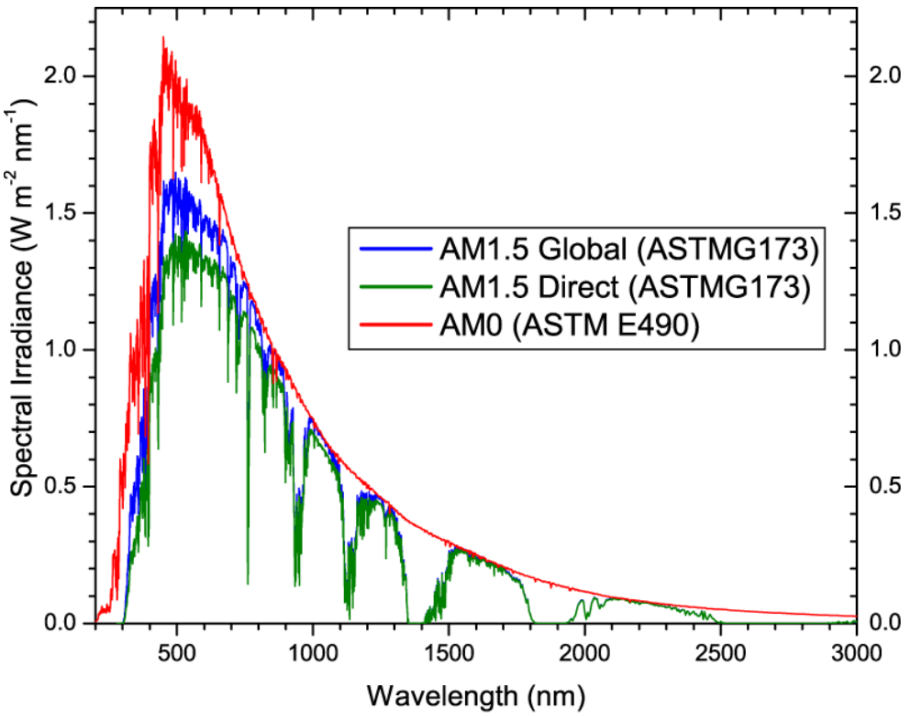

Fig. 1. Standard solar spectra for space and terrestrial use.

In this study, the core methodology is to obtain the devices' J_{SC}s and using that estimate their corresponding PCEs. By that, one can compare the multijunction device performances under the terrestrial and extraterrestrial test conditions.

The core device equation used is the following:-

$$J_{SC} = q \int_{spectrum} \boldsymbol{\phi}(\lambda) * EQE_{PV}(\lambda) * d\lambda, \text{ where}$$

$$\boldsymbol{\phi}(\lambda) = \frac{G(\lambda)*\lambda}{h*c}.$$

The power conversion efficiency (PCE) of the solar cell device is given as:-

$$PCE = \frac{P_{out}}{P_{in}} = \frac{V_{OC}*J_{SC}*FF}{P_{in}}.$$

In the given equation for J_{SC}, q is the electron charge, $\boldsymbol{\phi}(\lambda)$ is the incoming photon flux, $EQE_{PV}(\lambda)$ is the device's external quantum efficiency, and the integral of $\boldsymbol{\phi}(\lambda)$ modulated by $EQE_{PV}(\lambda)$ over the complete spectrum gives the essential device parameter J_{SC}. Further, the photon flux $\boldsymbol{\phi}(\lambda)$ is given by dividing the spectral irradiance (G(λ)) by the photon energy (hc/λ), λ being the wavelength, h the Planck constant and c the speed of light. The PCE is given as the ratio of output power (P_{out}) to input power (P_{in}), where Pout is given as the multiplication of open-circuit voltage (V_{OC}), short-circuit current (J_{SC}), and fill factor (FF).[18]

A numerical simulation was performed based on the above-given formula using a Python code involving interpolation and integration (using libraries like pandas, numpy, and matplotlib), where the spectral flux and the device's EQE_{PV} data were entered as data frames from the literature. EQE_{PV} data for the above-mentioned devices was obtained, with spectra digitized by manually extracting x and y values for different wavelengths ensuring an accurate representation of spectral features. The raw EQE_{PV} data was compiled into a CSV file and uploaded to a GitHub repository. In Python, interpolation techniques were employed to establish one data point per nm for both the EQE_{PV} and spectral data retrieved from GitHub. After converting the AM1.5G and AM0 spectral data to a photon flux, the product of EQE_{PV} and the photon flux were calculated. This gave the electron flux which was further transformed into current by integration to derive J_{SC} in A/m². Utilizing literature values for fill factor and V_{OC}, PCE was estimated. The process was repeated for all the devices, and their efficiencies were compared against literature PCE values, providing insights into the agreement between the performed numerical simulation and the literature.

RESULTS AND DISCUSSION

Novel halide segregation stable wide-bandgap perovskite

Using the literature, the EQE data for the mentioned devices were collected and plotted using our Python code-based numerical simulation. First of all, using the numerical simulation, the current spectra for the light-induced phase segregation suppressed 2.0 eV wide-bandgap

perovskite ($Rb_{0.15}Cs_{0.85}PbI_{1.75}Br_{1.25}$) based solar cell device introduced by Wang et al. are generated and compared to that of the contemporary 2.0 eV perovskite, $CsPbI_{1.4}Br_{1.6}$.

In Fig. 2, the quantum efficiency of the Rb/Cs mixed perovskite-based device is observed to be higher than that of the Cs-based perovskite. Simulating these solar cell devices under standard AM1.5G and AM0 conditions reveals that the Rb/Cs mixed perovskite-based device with an integrated J_{SC} 10.404 mA/cm^2 (under AM1.5G) and 13.552 mA/cm^2 (under AM0) consequently outperforms the Cs-based perovskite with 9.092 mA/cm^2 (under AM1.5G) and 11.508 mA/cm^2 (under AM0). Furthermore, the V_{OC} (1.3 V) and fill factor (79%) values for both devices are approximately the same, which means that the Rb/Cs mixed perovskite is more efficient (by approximately 1.5%) than the other. Thus, the Rb/Cs mixed perovskite, stable to phase segregation, proves to be a superior choice for the top cell absorber of a multijunction solar cell device in terrestrial and extraterrestrial conditions.

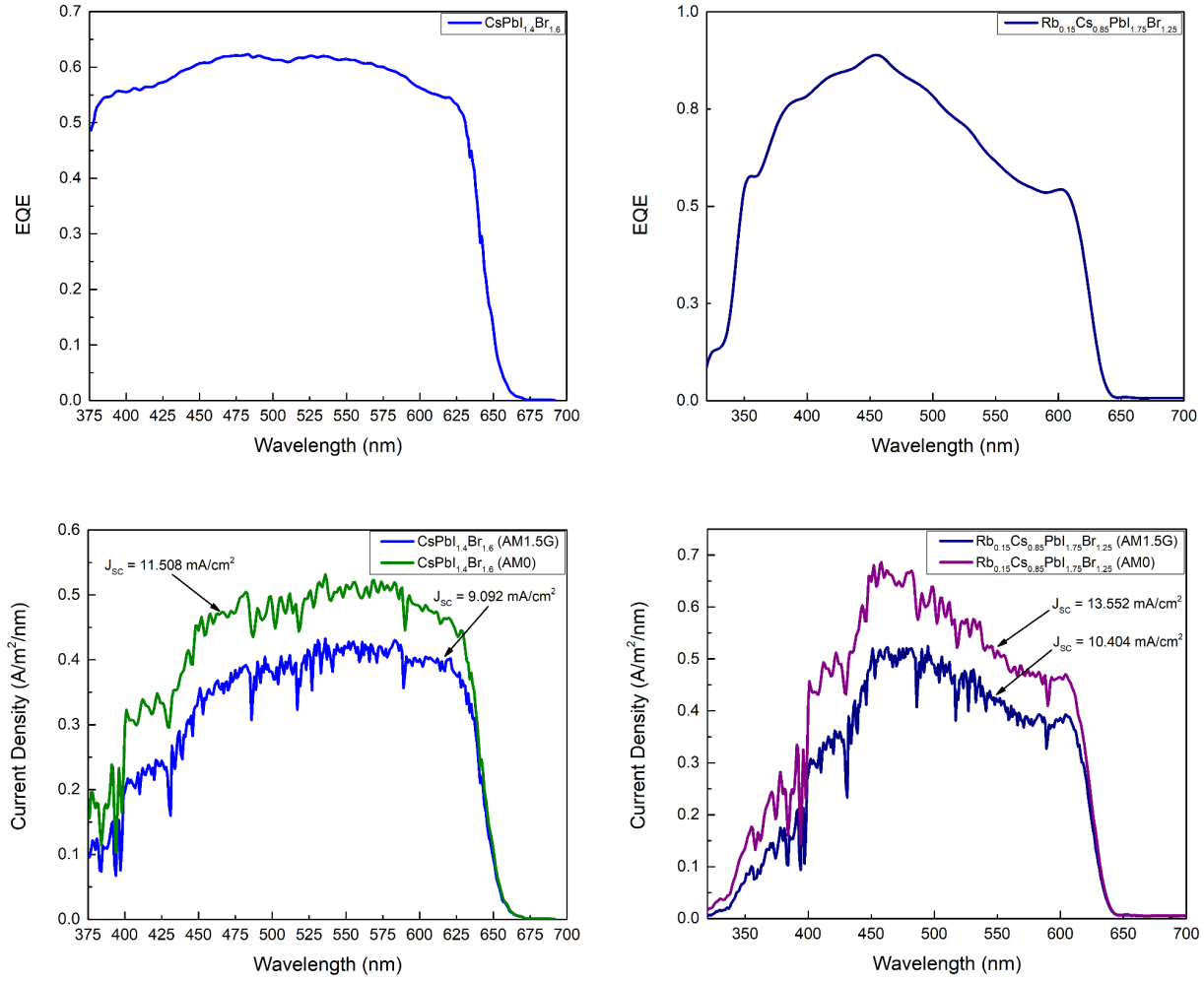

Fig. 2. EQE spectra comparison for $CsPbI_{1.4}Br_{1.6}$, and $Rb_{0.15}Cs_{0.85}PbI_{1.75}Br_{1.25}$ (top right and left), and their current spectra comparison under AM1.5G and AM0 (bottom right and left).

Widely-used 3J III-V vs. novel 3J perovskite solar cells

The EQE spectra for the triple junction III-V and perovskite devices are shown in Fig. 3. It is obvious that the incident photon conversion efficiency of the III-V multijunction device is higher than that of the perovskite multijunction device. This observation qualitatively suggests the superiority of the triple junction $Ga_{0.50}In_{0.50}P/Ga_{0.99}In_{0.01}As/Ge$ over the triple junction 2-eV Rb-Cs mixed-halide perovskite/1.6-eV perovskite/1.22-eV Sn-Pb mixed perovskite in terms of efficiency. Furthermore, the EQE of the III-V multijunction device outperforms in the context of the broad EQE spectra of the subcells, given the superior bandgaps of the junctions, especially the bottom subcell Ge (0.7 eV) compared to the 1.22 eV Sn-Pb mixed perovskite. Particularly, for the space standard test spectra (AM0) with no absorption in the IR regions, unlike AM1.5G spectra where atmospheric water vapour and carbon dioxide molecules absorb a huge part of the IR region of the spectra, the broadness of the EQE of the bottom cells are advantageous and desirable.

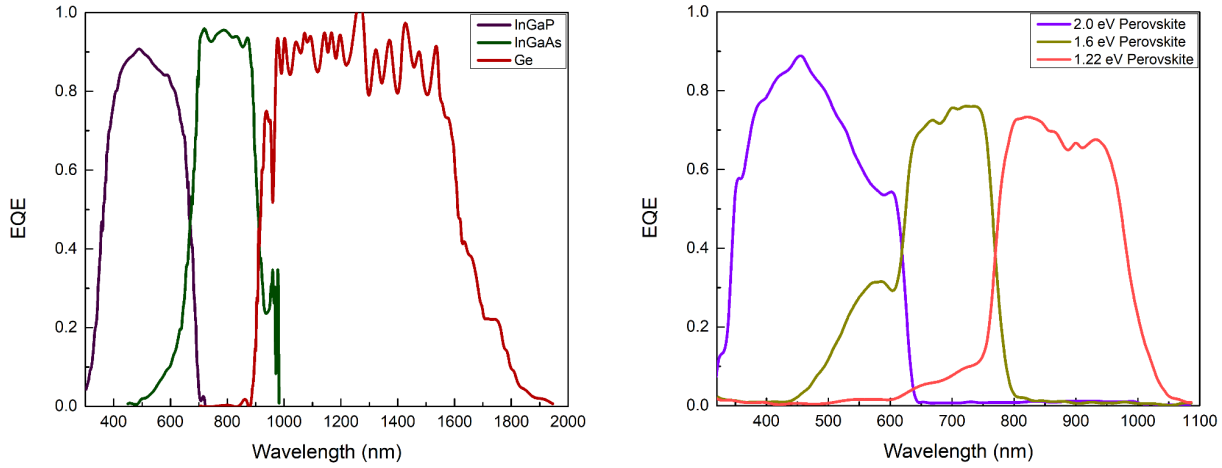

Fig. 3. Comparison of the EQE spectra for the $Ga_{0.50}In_{0.50}P/Ga_{0.99}In_{0.01}As/Ge$ (left) and the (2-eV Rb-Cs mixed-halide perovskite)/(1.6-eV perovskite)/(1.22-eV Sn-Pb mixed perovskite) (right).

The quantitative simulation analysis for the J_{SC} values for the subcells of the multijunction devices through the current spectra is shown in Fig. 4. As discussed earlier the V_{OC} of a 2-terminal multijunction solar cell device is the summation of the V_{OC}s of its subcells and the J_{SC} is the minimum of the subcells' J_{SC}s, according to Kirchoff's laws. In the given Fig. 4., the subcells of the multijunction devices are compared side by side. It can be seen that the subcells' integrated J_{SC} values for the III-V device exceed those of the all-perovskite device under AM1.5G and AM0 standard test conditions.

As discussed above, the bottom subcell of the III-V multijunction solar cell outperforms in terms of integrated J_{SC} significantly due to its broad and high EQE spectra compared to that of the all-perovskite multijunction solar cell. The top and middle subcells of the III-V triple junction device with absorber bandgaps of 1.8 and 1.42 eV respectively are better in terms of the integrated J_{SC} values than the 2.0 eV and 1.6 eV perovskite subcells of the triple junction perovskite solar cell.

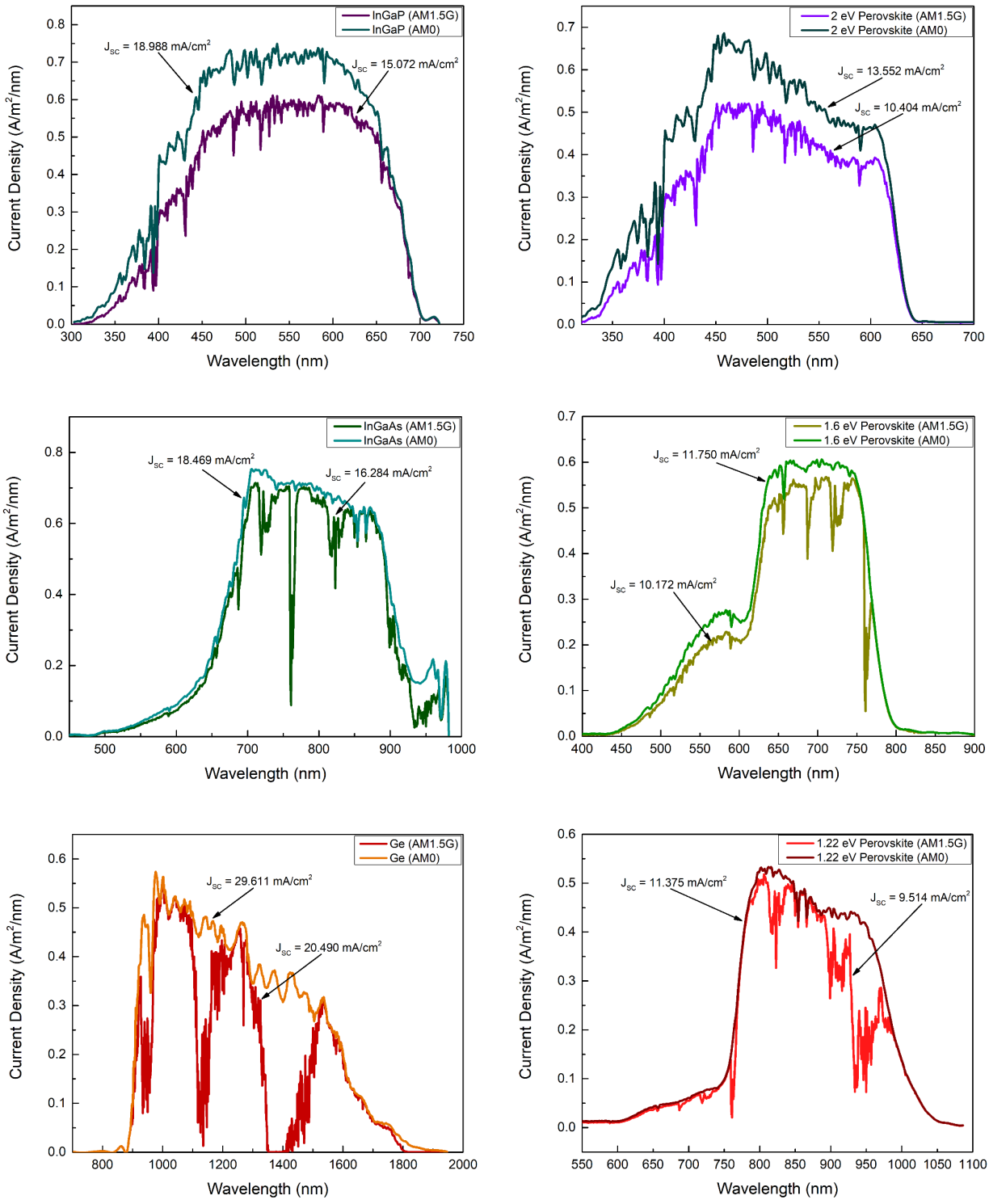

Fig. 4. Comparison of the current spectra of the three subcells of the 3J III-V-based solar cell and the novel halide segregation stable 3J perovskite solar cell. The figures on the left are for the subcells of the 3J III-V-based device and the figures on the right are those of the novel 3J perovskite-based device.

In terms of multijunction solar cell device efficiency, the values of V_{OC} and fill factor of the III-V-based device based on the literature are 2.54 V and 77% while that of the all-perovskite-based device are 3.2 V and 76.2% respectively. According to the numerical simulation performed in this work, the minimum J_{SC} of the III-V triple junction solar cell is 15.072 mA/cm^2 and that of the all-perovskite triple junction solar cell is 9.514 mA/cm^2, and hence the multijunction devices' PCEs come out to be approximately 30% and 23.2% respectively. It is hence quantitatively validated that the III-V multijunction solar cell is more efficient than the all-perovskite multijunction solar cell. The values of integrated J_{SC} as an outcome of the numerical simulations and the calculated values of PCEs are in proximity to the values specified in the literature.

CONCLUSION

The groundbreaking wide-bandgap perovskite, $Rb_{0.15}Cs_{0.85}PbI_{1.75}Br_{1.25}$, introduced by Wang et al., emerges as the optimal choice for the top subcell in all-perovskite multijunction solar cells, showcasing remarkable efficiency and robust stability against halide segregation. This novel inorganic perovskite material holds the potential to replace conventional inorganic wide-bandgap perovskites in multijunction applications, both on Earth and in extraterrestrial conditions. Although the all-perovskite multijunction device, fortified with the halide segregation-suppressed top cell absorber, excels in stability, it faces efficiency challenges when compared to III-V multijunction solar cell technologies. The III-V semiconductors, while sophisticated and robust, are hindered by their manufacturing intricacies, rigidity, thickness, and weight—qualities in stark contrast to the lightweight and versatile nature of perovskites, making them ideally suited for space applications. However, unlocking the full potential of all-perovskite multijunction solar cells requires meticulous device-specific research. This entails optimizing efficiencies by reducing bulk and interface trap state densities, minimizing parasitic absorption, and mitigating thin-film interference effects.[9] In the current landscape of space missions, which has seen the privatization of these endeavors, there is a substantial need for more cost-effective solar cell technologies and all-perovskite multijunction solar cells emerge as a promising candidate, offering a bright future for space-centric solar cell technologies.

REFERENCES

[1] R. Verduci, V. Romano, G. Brunetti, N. Yaghoobi Nia, A. Di Carlo, G. D'Angelo, and C. Ciminelli, "Solar Energy in Space Applications: Review and Technology Perspectives," Adv. Energy Mater. **12**(29), 2200125 (2022).

[2] W. Shockley, and H.J. Queisser, "Detailed Balance Limit of Efficiency of p-n Junction Solar Cells," J. Appl. Phys. **32**(3), 510–519 (2004).

[3] M. Yamaguchi, F. Dimroth, J.F. Geisz, and N.J. Ekins-Daukes, "Multi-junction solar cells paving the way for super high-efficiency," J. Appl. Phys. **129**(24), 240901 (2021).

[4] J. Li, A. Aierken, Y. Liu, Y. Zhuang, X. Yang, J.H. Mo, R.K. Fan, Q.Y. Chen, S.Y. Zhang, Y.M. Huang, and Q. Zhang, "A Brief Review of High Efficiency III-V Solar Cells for Space

Application," Front. Phys. **8**, (2021).

[5] M.A. Green, E.D. Dunlop, M. Yoshita, N. Kopidakis, K. Bothe, G. Siefer, and X. Hao, "Solar cell efficiency tables (version 62)," Prog. Photovolt. Res. Appl. **31**(7), 651–663 (2023).

[6] G.E. Eperon, M.T. Hörantner, and H.J. Snaith, "Metal halide perovskite tandem and multiple-junction photovoltaics," Nat. Rev. Chem. **1**(12), 1–18 (2017).

[7] F. Lang, G.E. Eperon, K. Frohna, E.M. Tennyson, A. Al-Ashouri, G. Kourkafas, J. Bundesmann, A. Denker, K.G. West, L.C. Hirst, H.-C. Neitzert, and S.D. Stranks, "Proton-Radiation Tolerant All-Perovskite Multijunction Solar Cells," Adv. Energy Mater. **11**(41), 2102246 (2021).

[8] J. Albero, A. M. Asiri, and H. García, "Influence of the composition of hybrid perovskites on their performance in solar cells," J. Mater. Chem. A **4**(12), 4353–4364 (2016).

[9] M.T. Hörantner, T. Leijtens, M.E. Ziffer, G.E. Eperon, M.G. Christoforo, M.D. McGehee, and H.J. Snaith, "The Potential of Multijunction Perovskite Solar Cells," ACS Energy Lett. **2**(10), 2506–2513 (2017).

[10] S. Mahesh, J.M. Ball, R.D.J. Oliver, D.P. McMeekin, P.K. Nayak, M.B. Johnston, and H.J. Snaith, "Revealing the origin of voltage loss in mixed-halide perovskite solar cells," Energy Environ. Sci. **13**(1), 258–267 (2020).

[11] E.T. Hoke, D.J. Slotcavage, E.R. Dohner, A.R. Bowring, H.I. Karunadasa, and M.D. McGehee, "Reversible photo-induced trap formation in mixed-halide hybrid perovskites for photovoltaics," Chem. Sci. **6**(1), 613–617 (2014).

[12] A.J. Ramadan, R.D.J. Oliver, M.B. Johnston, and H.J. Snaith, "Methylammonium-free wide-bandgap metal halide perovskites for tandem photovoltaics," Nat. Rev. Mater., 1–17 (2023).

[13] B. Yu, S. Tan, D. Li, and Q. Meng, "The stability of inorganic perovskite solar cells: from materials to devices," Mater. Futur. **2**(3), 032101 (2023).

[14] Z. Wang, L. Zeng, T. Zhu, H. Chen, B. Chen, D.J. Kubicki, A. Balvanz, C. Li, A. Maxwell, E. Ugur, R. dos Reis, M. Cheng, G. Yang, B. Subedi, D. Luo, J. Hu, J. Wang, S. Teale, S. Mahesh, S. Wang, S. Hu, E.D. Jung, M. Wei, S.M. Park, L. Grater, E. Aydin, Z. Song, N.J. Podraza, Z.-H. Lu, J. Huang, V.P. Dravid, S. De Wolf, Y. Yan, M. Grätzel, M.G. Kanatzidis, and E.H. Sargent, "Suppressed phase segregation for triple-junction perovskite solar cells," Nature **618**(7963), 74–79 (2023).

[15] R.E. Beal, D.J. Slotcavage, T. Leijtens, A.R. Bowring, R.A. Belisle, W.H. Nguyen, G.F. Burkhard, E.T. Hoke, and M.D. McGehee, "Cesium Lead Halide Perovskites with Improved Stability for Tandem Solar Cells," J. Phys. Chem. Lett. **7**(5), 746–751 (2016).

[16] C.A. Gueymard, "Revised composite extraterrestrial spectrum based on recent solar irradiance observations," Sol. Energy **169**, 434–440 (2018).

[17] G03 Committee, *Tables for Reference Solar Spectral Irradiances: Direct Normal and*

Hemispherical on 37 Tilted Surface (ASTM International, n.d.).

[18] J. Bisquert, *The Physics of Solar Cells: Perovskites, Organics, and Photovoltaic Fundamentals* (CRC Press, 2017).

SUPPORTING INFORMATION AND DATA

1. AM1.5G and AM0 data:
   https://github.com/FotoVoltz/PV_Systems/raw/main/AM0AM1_5.xls
2. EQE spectral data for the devices were taken from the literature as given below:-
   A. $CsPbI_{1.4}Br_{1.6}$ based solar cell:
      https://doi.org/10.1021/acs.jpclett.6b00002
   B. $Rb_{0.15}Cs_{0.85}PbI_{1.75}Br_{1.25}$ based solar cell:
      https://doi.org/10.1038/s41586-023-06006-7
   C. $Ga_{0.50}In_{0.50}P/Ga_{0.99}In_{0.01}As$/Ge triple junction solar cell:
      https://doi.org/10.1109/PVSC.2010.5614525
   D. $Rb_{0.15}Cs_{0.85}PbI_{1.75}Br_{1.25}$ WBG semiconductor-based triple junction solar cell:
      https://doi.org/10.1038/s41586-023-06006-7
3. Python Code for the Numerical Simulation:
   https://colab.research.google.com/drive/1OoPjUzq7xCEpWNoG7YYYvo2zdNEe_KAZ?usp=sharing